

Research papers

Hydrogen absorption-desorption properties and hydrolysis performance of $\text{MgH}_2\text{-Zr}_3\text{V}_3\text{O}_{0.6}\text{H}_x$ and $\text{MgH}_2\text{-Zr}_3\text{V}_3\text{O}_{0.6}\text{H}_x\text{-C}$ composites

Ihor Zavaliiy^{a,*}, Vasyl Berezovets^a, Roman Denys^b, Oleksandr Kononiuk^a, Volodymyr Yartys^c

^a Physico-Mechanical Institute of the NAS of Ukraine, 5, Naukova str., 79060 Lviv, Ukraine

^b HYSTORSYS AS, P.O. Box 45, Kjeller NO-2027, Norway

^c Institute for Energy Technology, P.O. Box 40, N-2027 Kjeller, Norway



ARTICLE INFO

Keywords:

Magnesium composites

Hydrogen storage

Hydrogen sorption-desorption properties

ABSTRACT

In this work, the catalytic effect of additions of $\eta\text{-Zr}_3\text{V}_3\text{O}_{0.6}$ mixed suboxide and the title intermetallic composite with graphite on the properties of MgH_2 in the processes of hydrogen storage and hydrogen generation has been studied. The hydride composites were obtained by high-energy reactive ball milling (RBM). The samples were characterized by X-ray diffraction and scanning electron microscopy. The cycling performance of hydrogen desorption and absorption as well as hydrogen generation in the hydrolysis reaction were studied. We found that during the reactive ball milling the studied composites are able in a few minutes to absorb ~ 6.5 wt% of hydrogen. The addition of $\text{Zr}_3\text{V}_3\text{O}_{0.6}$ and $\text{Zr}_3\text{V}_3\text{O}_{0.6} + \text{C}$ catalysts not only increases the rates of hydrogen absorption and release, but also lowers the activation energy and the temperature of hydrogen desorption. For a composite containing 10 wt% of suboxide and 3 wt% of graphite, the activation energy of hydrogen desorption determined by the Kissinger method was very low, just 58 kJ/mol, and this value is among the lowest described in the reference publications. We also show that the intermetallic additive forms the $\text{Zr}_3\text{V}_3\text{O}_{0.6}\text{H}_{\sim 10}$ hydride, which results in a higher gravimetric capacity of the composite as H storage material. The improved kinetics of hydrogen exchange and increased hydrogenation capacity at modest operating temperatures of 150–200 °C appear to be characteristic for the composites containing suboxide and graphite additions. The reason for the advanced performance is in the different the morphology of the synthesized samples, particularly the graphite-containing composites showing a more developed dispergation of the material (the fraction with a particle size of 1–3 μm is >80 wt%). We furthermore show that the synthesized materials can be used in the hydrolysis process resulting in hydrogen generation. The amount of hydrogen released from the hydride $\text{Mg-Zr}_3\text{V}_3\text{O}_{0.6}\text{-C}$ composite in the hydrolysis reaction reaches 1364 ml/g (the conversion degree is ~ 85 % for the process duration of 120 min) when using 0.04 M MgCl_2 solutions.

1. Introduction

The use of metal hydrides, which absorb and release hydrogen at convenient close-to-ambient conditions, is a convenient alternative to storing hydrogen as a compressed hydrogen gas. Magnesium hydride MgH_2 has a high energy density. However, its use meets a significant challenge as absorption-desorption of hydrogen occurs at inconveniently high temperatures exceeding 300 °C [1–3]. The hydrogenation of magnesium proceeds in several steps, including diffusion of H_2 molecules to the metal surface, chemisorption, dissociation of molecular H_2 to H atoms, diffusion of hydrogen atoms from the surface into the bulk, nucleation and growth of the hydride phase [4]. The clean surface of

magnesium is frequently insufficiently active to achieve the high rates of H_2 dissociation [5] and, therefore, the activation barrier of H_2 dissociation should be reduced by adding various catalysts thus increasing the rates of the process [2,6–11]. Furthermore, for magnesium metal the transformation $\text{Mg} \rightarrow \text{MgH}_2$ is slow due to the sluggish diffusion of hydrogen through the hydride layer. Therefore, the kinetics of sorption-desorption significantly depends on the size of the particles and their specific surface area [12]. The processes of hydride formation/decomposition can be accelerated by (1) facilitating the dissociation of H_2 molecules at the surface, (2) reducing the grain size (to shorten the paths for hydrogen diffusion) and (3) increasing the number of active centers for the nucleation of a formation of the hydride phase.

* Corresponding author.

E-mail address: ihor.zavaliiy@gmail.com (I. Zavaliiy).

<https://doi.org/10.1016/j.est.2023.107245>

Received 11 November 2022; Received in revised form 15 February 2023; Accepted 23 March 2023

Available online 6 April 2023

2352-152X/© 2023 The Authors. Published by Elsevier Ltd. This is an open access article under the CC BY-NC-ND license (<http://creativecommons.org/licenses/by-nc-nd/4.0/>).

It was known [3,12,13] that for the milled magnesium, hydrogen sorption kinetics is improved due to the microstructural changes: the depletion of the surface oxide layers, nanocrystallization of the alloy, and the formation of a large number of defects in hydrogen storage material. Microstructural defects act as centers of nucleation of the hydride phase, while increased areas of intergrain boundaries act as pathways for the quick hydrogen diffusion. Mechanochemical hydrogenation in hydrogen gas occurs at ambient temperature and makes it possible to achieve a complete conversion of magnesium into its hydride [3]. Recent reviews of the studies of magnesium-based hydrogen storage materials show that magnesium hydride remains an important topic for both fundamental research and practical applications [6–9,14]. However, further work is needed to evaluate the effectiveness of catalysts, which involves studies of intermetallic compounds and their effect on the hydrogenation behaviors of magnesium nanostructures. Various materials, including transition metals and their compounds (oxides, halides, borides, nitrides, carbides, hydrides, etc.), intermetallic compounds, and carbon materials were used to improve the hydrogenation properties of magnesium [15–33]. Among the catalysts, transition metals and their oxides most effectively affect the kinetics of hydrogenation-dehydrogenation of magnesium [9,20,24,25]. Particularly effective catalysts are Ti [27] and its hydrides TiH_{2-x} [19,34–39], or ZrH_2 [40]. As an example, $\text{Mg-TiH}_{1.971}\text{-TiH}_{1.5}$ nanocomposite at room temperature absorbed 4.3 wt% H_2 in 10 min [36]. In [41–43], the hydrogenation properties of magnesium were improved by using additives of intermetallic compounds and alloys (ZrFe_2 , ZrMn_2 , $\text{Zr}_{0.4}\text{Ti}_{0.6}\text{Co}$). An important feature of some mechanochemically synthesized Mg-based composites there is their re-hydrogenation at room temperature. It has been shown that this can be a consequence of composition of intermetallic compound as a catalyst [44], nano-size of catalytic additives (Ti, TiO_2) [45] or hard conditions of mechanochemical synthesis [38].

Hydrogenation behaviors of magnesium catalyzed by adding $\text{Ti}_4\text{Fe}_2\text{O}_x$ suboxides were studied in [45], while a better cyclic stability of these composites was obtained when graphite was used as an extra additive. The activation energy for the obtained composite (67 kJ/mol) was among the lowest described in the reference data. These data indicate that suboxides and their hydrides, in particular, the isostructural zirconium-based η -phase $\text{Zr}_3\text{V}_3\text{O}_x$ [46–48] may also show advanced catalytic performance.

One promising application of magnesium hydride is generation of hydrogen using hydrolysis process [49–57], followed by its further use in fuel cells. It has a number of advantages: high weight capacity of H, cost efficiency [52], non-toxicity [58], and extended storage life. Therefore, elaborating a quick and cost-efficient production of MgH_2 is very important for such a use. Unfortunately, the reaction rate is extremely slow. Attempts to increase the yield of hydrogen were all based on using additives of acids, salts, and an increase in the reaction temperature. Furthermore, significant improvement of the reaction kinetics can be achieved by employing the high-energy ball milling resulting in the formation of nanocrystalline MgH_2 [59]. Synthesis of magnesium hydride by mechanochemical milling is more efficient with the use of catalysts [45], as catalysts can reduce the reaction time by up to five times.

The dissociation of hydrogen molecules at the surface of magnesium metal is difficult to realize. However, the catalysts reduce the energy barrier of this process. Efficient catalysts also facilitate formation of hydrogen molecules from atomic H during hydrogen desorption from magnesium hydride. Among them, we highlight titanium hydride [34–39], titanium oxides [60,61] and niobium [19,22,62]. Furthermore, $\text{Ti}_4\text{Fe}_2\text{O}_x$ catalysts were recently described in [45] and showed a very low E_a . During the hydrogenation, the catalyst becomes a source of atomic hydrogen for the hydrogenation of magnesium. Finally, during desorption, the catalyst releases hydrogen at lower temperatures than those for MgH_2 . In this work, we selected as a catalyst the oxygen-containing intermetallic alloy $\text{Zr}_3\text{V}_3\text{O}_{0.6}$, which is a stabilized by oxygen compound with a Ti_2Ni -type structure and has similar hydrogen

sorption properties to $\text{Ti}_4\text{Fe}_2\text{O}_x$.

This work studies the influence of additives on the process of mechanochemical hydrogenation of magnesium. In particular, the effect of graphite and a hydride-forming $\text{Zr}_3\text{V}_3\text{O}_{0.6}$ compound on hydrogen sorption properties was studied. The hydrogen generation in the hydrolysis process for the synthesized composite materials, $\text{MgH}_2\text{-Zr}_3\text{V}_3\text{O}_{0.6}$ and $\text{MgH}_2\text{-Zr}_3\text{V}_3\text{O}_{0.6}\text{-C}$, was studied to assess possibilities of their used as efficient materials for the *in-situ* hydrogen generation.

2. Experimental

The starting components for the preparation of hydride nanocomposites were magnesium powder (Fluka, 99 + %) with a particle size of 0.1–0.3 mm, graphite powder ($\leq 20 \mu\text{m}$, Fluka, 99 + %), and compact $\text{Zr}_3\text{V}_3\text{O}_{0.6}$ alloy. $\text{Zr}_3\text{V}_3\text{O}_{0.6}$ alloy was prepared by arc melting in a purified argon atmosphere from high purity ($\geq 99.9\%$) compact metals and compressed ZrO_2 powder. The dissolution of ZrO_2 powder in the molten alloy was visually observed. The sample was remelted several times. The sample mass loss during the melting was $< 0.5\%$; thus, the composition of the prepared oxide was assumed to be defined by the stoichiometry of the mixture. As a result, the single phase $\text{Zr}_3\text{V}_3\text{O}_{0.6}$ intermetallic compound was obtained. The as-cast alloys were annealed in vacuum at 980°C for five days.

Magnesium-based hydride composites were prepared by reactive ball milling in a hydrogen gas using a Fritsch Pulverisette-6 planetary mill. The milling was carried out in a custom made 80 ml milling vial. The vial allowed milling under gas pressure up to 5 MPa. For gas input and output, the lid of the vial was equipped with two Swagelock needle valves. Stainless steel balls (30 balls with a diameter of 10 mm) were used as milling bodies. The ratio of the weight of milling bodies ($\approx 120 \text{g}$) to the weight of the sample was 60:1. The milling was carried out at a rotation speed of 500 rpm.

To control the process of mechanochemical hydrogenation of the sample, the milling was periodically paused (with an interval of 15–20 min), the vial, after cooling to room temperature, was connected to a Sieverts-type apparatus and the hydrogen pressure was measured using a pressure sensor (measurement accuracy 0.05 %). After that, hydrogen was added to the vial until the initial pressure (2 MPa) was reached and the milling process was continued. The amount of hydrogen absorbed by the sample in the reactive milling process was determined by the volumetric method based on the monitoring of the hydrogen pressure changes.

The hydrogen sorption properties of the hydride composites were studied using a Sieverts-type apparatus. The amount of absorbed/released hydrogen was determined by the volumetric method. Hydrogen desorption was carried out into a closed volume at a constant temperature (in the range from 275 to 375°C) under the initial hydrogen pressure of 0.05–0.1 MPa, while absorption was performed in a temperature range of 25 – 350°C under the initial hydrogen pressure of 2 MPa. Desorption of hydrogen by hydride nanocomposites was further studied by thermodesorption spectroscopy (TDS), by heating the sample with a constant rate ($2^\circ\text{C}/\text{min}$) in a dynamic vacuum from room temperature to 350 – 400°C .

The activation energy (E_a) of hydrogen desorption from the samples obtained by the ball milling was studied by Thermal Desorption Spectroscopy (TDS). 50–70 mg of the sample were loaded into the reactor, which was pumped at room temperature to a pressure of $< 10^{-3}$ Pa. TDS measurements were performed by heating the reactor at a constant heating rate of 0.5 – 5K min^{-1} from room temperature to 325°C under dynamic vacuum conditions. The release of H_2 leads to an increase in the pressure in the system, which was monitored by the vacuum sensor. The activation energy of hydrogen desorption was determined by Kissinger method [63] using the equation given in [39]. For the sample containing carbon, the rehydrogenation was carried out at 200°C and a pressure of 1.5 MPa.

X-ray diffraction studies of the samples were based on the data

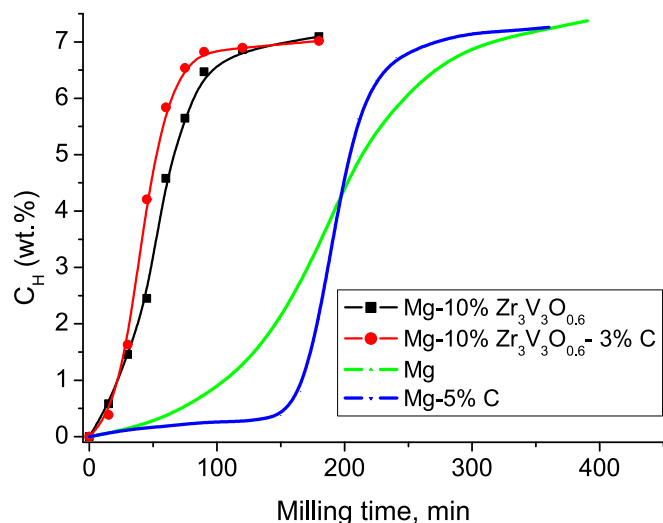


Fig. 1. Curves of mechanochemical hydrogenation of the mixtures of magnesium, $Zr_3V_3O_{0.6}$ alloy, and graphite (2 MPa H_2). The data for Mg and Mg-5% C are taken from the reference [39].

Table 1

Kinetic parameters of the process of mechanochemical hydrogenation of Mg and Mg-based mixtures.

Composition	K, min^{-1}	$C_{H\text{max}}, \text{wt}\%$	n
Mg ^a	0.00486(6)	7.36	3.1(1)
Mg-5 wt% C ^a	0.016(4)	7.28	2.6(7)
90 wt% Mg-10 wt% $Zr_3V_3O_{0.6}$	0.0165(5)	7.04	2.25(18)
87 wt% Mg-10 wt% $Zr_3V_3O_{0.6}$ -3 wt% C	0.0213(3)	6.88	2.68(14)

^a Reference [39].

collected using a DRON-3.0 powder diffractometer (Cu-K α radiation). Powder diffraction data was analyzed by Rietveld full-profile refinement method using the GSAS (General Structure Analysis System) software package [64]. The shape of the peaks was described using the pseudo-Voigt function of Thompson-Coggs-Hastings [65].

The size of the crystallites and the level of microstresses in the materials were estimated from the profile parameters refined the Rietveld method, using the following equations [66]: $D_V = \lambda / (\beta_s \cdot \cos\theta)$; $e = \beta_D / (4 \cdot \tan\theta)$, where D_V is the volume-weighted size of crystallites; e is microstress; λ is the wavelength of X-ray radiation; β_s and β_D – are the integral widths of the diffraction peaks, calculated from the profile parameters that take into account the contribution to the peak width from

the size of the crystallites and microstresses, respectively; θ – is the Bragg angle. The instrumental contribution to the width of the X-ray peaks was determined using the refinement of the profile parameters for the diffraction pattern of a silicon powder used as a standard.

3. Results and discussion

3.1. Synthesis of Mg- $Zr_3V_3O_{0.6}$ and Mg- $Zr_3V_3O_{0.6}$ -graphite hydride composites

Magnesium hydride composites containing 10 wt% of the hydride-forming η -phase $Zr_3V_3O_{0.6}$, as well as a ternary composite with an addition of 3 wt% graphite, were synthesized by the reactive milling in hydrogen. Fig. 1 shows the hydrogenation curve of a mixture of magnesium powder with the addition of $Zr_3V_3O_{0.6}$ alloy under a hydrogen pressure of 2 MPa. Similar to pure magnesium, the dependence of the hydrogen sorption capacity on the milling time has a sigmoidal shape, but the rate of hydrogenation is almost three times higher, which indicates the catalytic effect of $Zr_3V_3O_{0.6}$. Complete saturation of the composite material with hydrogen (maximum capacity 7.0 wt% H) occurs in <2 h of milling. The rate of the hydrogenation of the Mg-10 wt% $Zr_3V_3O_{0.6}$ mixture is also significantly higher than that of magnesium-graphite mixtures [67] (see Fig. 1). Addition of graphite improves kinetics, however the saturation time remains practically the same as for magnesium studied without graphite additives, due to a long induction period of the mechanochemical hydrogenation process. The addition of 3 wt% graphite to the Mg- $Zr_3V_3O_{0.6}$ mixture leads to a further increase of the rate of process of mechanochemical hydrogenation (Fig. 1 and Table 1). Thus, we observe a synergistic effect of intermetallic compound and graphite. A similar effect was observed in previous studies for the mixtures Mg-20%Ti₄Fe₂O_{0.5}-5% C [45] and Mg-10% V₇₅Ti₁₀Zr_{7.5}Cr_{7.5}-5% C [15]. It should also be noted that in the presence of intermetallic compound, the induction period of hydrogenation caused by the addition of graphite disappears.

The hydrogen absorption curves for Mg with additions of oxygen-stabilized η -phase $Zr_3V_3O_{0.6}$ and the ternary Mg- $Zr_3V_3O_{0.6}$ -C composite obtained during reactive milling are presented in Fig. 1. The hydrogenation is completed in 1–1.5 h and the hydrogen capacity of the formed hydride composites is 6.5 wt%.

The presence of $Zr_3V_3O_{0.6}$ leads to 3–4 times increase in the reaction rate constant. The Avrami exponent is 2.25 and 2.68 for the composite without/with carbon, respectively. This indicates that the rate of the phase transformation is the rate limiting step of the process ($n = 2$ or 3, depending on the mechanism of nucleation and growth of the hydride phase) [68]. A similar mechanism of catalysis was observed for the Ti₄Fe₂O_{0.3} suboxides [45], while nano-Ti and nano-TiO₂ force a

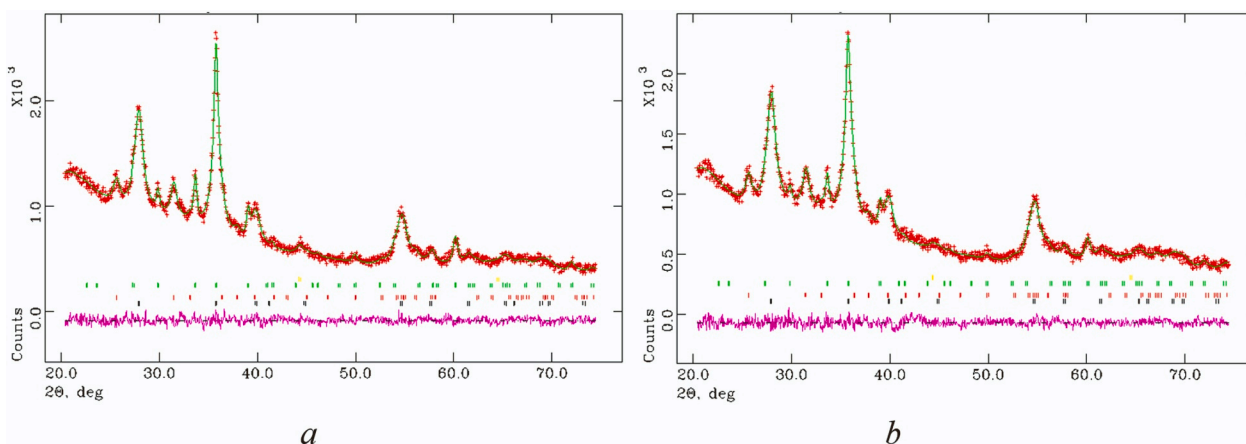
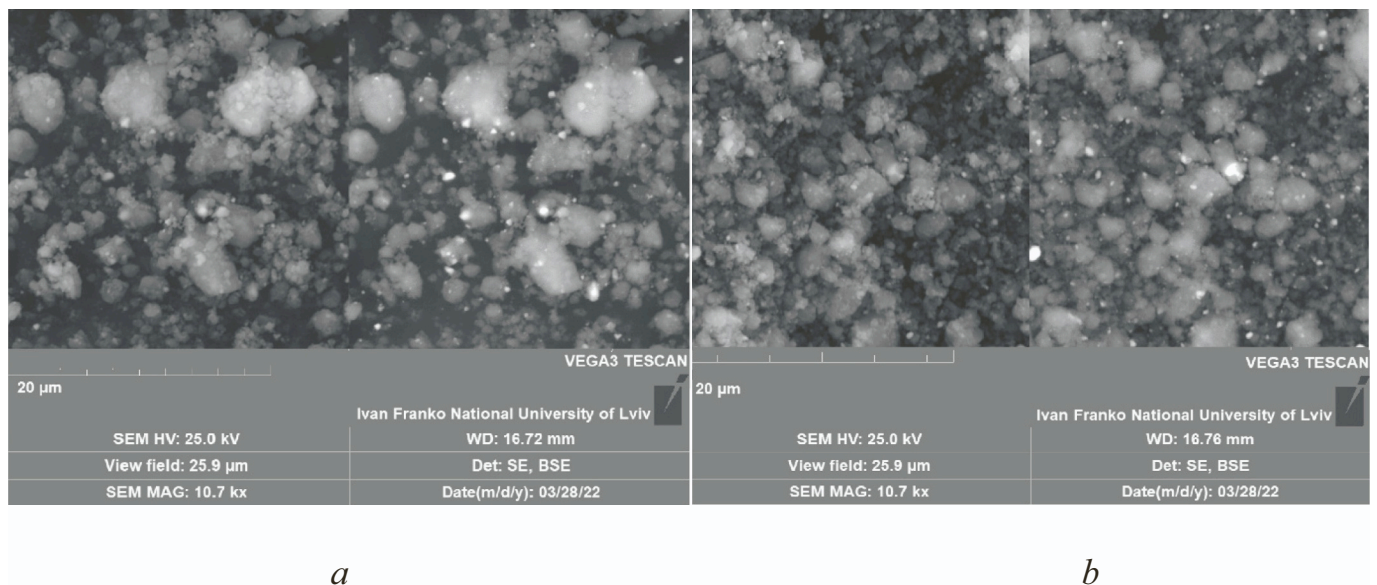


Fig. 2. Experimental (+), calculated (–) and difference (bottom line) diffraction profiles of the hydrogenated composites: (a) Mg-10% $Zr_3V_3O_{0.6}$ and (b) Mg-10% $Zr_3V_3O_{0.6}$ -3% C. Vertical lines (|) show the positions of the peaks of the component phases (from bottom to top): α -MgH₂, γ -MgH₂, $Zr_3V_3O_{0.6}H_{-10}$, and α -Fe.

Table 2

Phase-structural characteristics of the materials from the Rietveld refinements data after the mechano-chemical hydrogenation.

Material	Phase	Space group	Lattice parameters, Å	Content, wt%	Sizes of crystallites (D_V); microstress (e)
90%Mg-10%Zr ₃ V ₃ O _{0.6}	α -MgH ₂	$P4_2/mnm$	$a = 4.522(1) \ c = 3.017(1)$	71.1(1)	$D_V = 9.6(3) \text{ nm}$ $e = 0.92(4) \%$
	γ -MgH ₂	$Pbcn$	$a = 4.539(3) \ b = 5.412(5)$ $c = 4.938(6)$	19.5(3)	$D_V = 9.0(3) \text{ nm}$ $e = 0.1(-) \%$
	Zr ₃ V ₃ O _{0.6} H ₋₁₀	$Fd\bar{3}m$	$a = 13.052(2)$	8.4(1)	–
	α -Fe	$Im\bar{3}m$	$a = 2.890(4)$	1.0(1)	–
87%Mg-10%Zr ₃ V ₃ O _{0.6} -3%C	α -MgH ₂	$P4_2/mnm$	$a = 4.519(1) \ c = 3.020(1)$	72.6(2)	$D_V = 8.7(6) \text{ nm}$ $e = 0.83(9) \%$
	γ -MgH ₂	$Pbcn$	$a = 4.532(4) \ b = 5.424(5)$ $c = 4.948(8)$	19.9(5)	$D_V = 8.9(5) \text{ nm}$ $e = 0.1(-) \%$
	Zr ₃ V ₃ O _{0.6} H ₋₁₀	$Fd\bar{3}m$	$a = 13.065(2)$	7.0(1)	–
	α -Fe	$Im\bar{3}m$	$a = 2.891(6)$	0.5(1)	–

**Fig. 3.** Microstructure of hydride composites: Mg-10%Zr₃V₃O_{0.6} (a) and Mg-10%Zr₃V₃O_{0.6}-3%C (b).

different reaction mechanism ($n \sim 1.5$) where H diffusion is the limiting stage [39,45]. It is known that the rate of hydrogenation during the ball milling depends on both the rate of nucleation of magnesium hydride crystallization centers and the rate of diffusion through the formed hydride layer. It is obvious that these processes are influenced by the addition of appropriate catalysts. Analysis of the shape of hydrogen absorption curves (Fig. 1), for the composites with added catalyst and with a catalyst and carbon, shows that in both cases the limiting stage of the hydrogenation is the nucleation of the new centers of crystallization (Avraami exponent is 2.25 and 2.68). Based on this, we assume that the role of carbon is in preventing the agglomeration of magnesium hydride particles during the ball milling. This explains the smaller particle size that is observed in the case of carbon composite.

3.2. Phase composition and morphology of the synthesized composites

The X-ray diffraction pattern of the samples after the high-energy milling in hydrogen is very similar to each other (see Fig. 2) and indicate a complete transformation of magnesium and IMC into the corresponding hydrides. The phase compositions of the composites according to the results of the Rietveld refinements are given in Table 2. During the mechanochemical hydrogenation, Zr₃V₃O_{0.6} preserves its original type of structure. The formation of the saturated hydride Zr₃V₃O_{0.6}H₋₁₀ causes the expansion of the unit cell, $\Delta V/V_{IMC} = 26 \%$. No other components were found. The appearance of traces of iron (<1 wt%) is caused by the abrasion of milling bodies during the high-energy milling.

Occasionally, magnesium oxide was also observed, formed due to a slight oxidation of the formed material.

The microstructure of composite hydrides synthesized by mechano-chemical milling was studied by using scanning electron microscopy and is shown in Fig. 3. The micrographs of the composite hydrides show that the graphite additions cause a formation of smaller particles. It can be seen that the sizes of the obtained particles are in the range from ~ 50 nm to several micrometers. The size of particles was evaluated also using an AxiVision V 4.8.2.0 (Carl Zeiss Microscopy) software (see Supplementary Information file (SI), part S1). The particle size distribution in these composites and the approximate weight fractions of particles of a certain size are shown in Fig. 4 and Table 3. The main fraction are the particles with size $>3 \mu\text{m}$ (77 wt%) for the Mg-Zr₃V₃O_{0.6} hydride composite, while the fraction with a particle size of 1–3 μm is 80 wt% for the hydride composite with graphite.

3.3. Dehydrogenation and rehydrogenation of the synthesized composites

Desorption from hydride composites was carried out into a dynamic vacuum and a closed volume where a certain initial hydrogen pressure was maintained. Curves of vacuum thermodesorption (TDS) of hydrogen from hydride composites Mg-10%Zr₃V₃O_{0.6}, Mg-10%Zr₃V₃O_{0.6}-3%C, and nanocrystalline magnesium hydride (for comparison) after mechanochemical milling in hydrogen are shown in Fig. 5.

Desorption of hydrogen from both composite materials occurs in the temperature range of 150–300 °C with a peak at ~ 235 °C, which is 70 °C

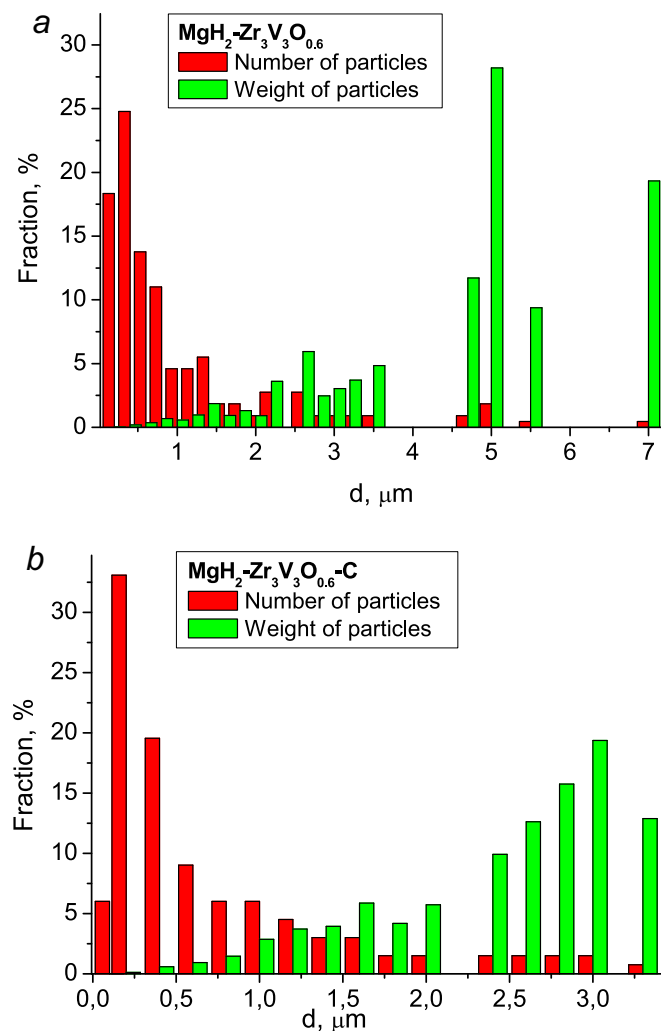


Fig. 4. Size distributions of the particles in the synthesized composites.

Table 3
Size distributions of the particles in the prepared composites.

Fraction of particles, μm	90%Mg-10%Zr ₃ V ₃ O _{0.6}		87%Mg-10%Zr ₃ V ₃ O _{0.6} -3%C	
	Number, %	Wt., %	Number, %	Wt., %
0.1–1	72.5	1.8	79.7	6.0
1–3	22.0	21.1	19.5	81.1
>3	5.5	77.1	0.8	12.9

lower than the peak temperature of thermal desorption from the nanocrystalline magnesium hydride. Such a significant shift of the TDS peak indicates an improvement in the kinetics of magnesium hydride decomposition and a decrease in the activation energy of desorption due to the catalytic effect of the η -phase. In contrast, the decomposition peak of magnesium-graphite hydride composites is only $\sim 10^\circ\text{C}$ lower than the peak of magnesium hydride. For the Mg–10 % Zr₃V₃O_{0.6} composite, a splitting of the TDS peak is observed, which becomes more pronounced after rehydrogenation of the composite by the traditional method at a temperature of 200 °C under a hydrogen pressure of 2 MPa (Fig. 5b). Such splitting can be explained by distribution of the material particle sizes, since a similar bifurcation of the TDS peak was also observed for unmodified nanocrystalline magnesium hydride [69–71]. The study of the morphology of the Mg–Zr₃V₃O_{0.6} composite also showed a rather uneven distribution of the particles in terms of size. In the sample without carbon, the weight fraction of particles >3 μm in size is 77 %,

whereas in one with carbon, the distribution is more uniform, and particles of this size are practically absent (Table 3, SI part S1). We note that in the composite with graphite (Mg–10%Zr₃V₃O_{0.6}-3%C), the bifurcation of the desorption peak is not observed, probably due to a more uniform distribution of the particle sizes of the material.

The fact that the thermal desorption peak bifurcates for the samples that do not contain carbon is interesting. The reason for this may be the presence of particles of variable sizes with different surface-to-bulk ratio in the sample. The first peak corresponds to the release of hydrogen from smaller particles (higher surface-to-bulk ratio) which overlaps with the event of H₂ desorption from the near-surface layer of larger particles. In contrast, the second peak corresponds to the release of hydrogen from the core of larger particles, when a diffusion path is longer. The intensity and half-width of these peaks changes during repeated cycles of hydrogenation-dehydrogenation, and only one peak is observed after ten cycles of hydrogen absorption-desorption.

We also assured during the measurements a sufficiently high thermal conductivity in the sample, enabling its even heating. The temperature gradient of the autoclave was negligible. Thus, it became possible to prevent sublimation and deposition of magnesium at the colder part of the autoclave. Finally, no new phases, which could become a surface barrier to hydrogen release, were formed, as confirmed by X-ray analysis.

Desorption of hydrogen at 350 °C under initial pressure in the gas system of 0.17 MPa from the freshly prepared hydride composites by reactive milling occurs within 3 min, and the amount of hydrogen released exceeds 6 wt% (SI part S2, Fig. S2-1). After 5 cycles of hydrogen absorption-desorption at a temperature of 350 °C, the reversible hydrogen sorption capacity is preserved, and the kinetics of the desorption process even improves: Mg–10 % Zr₃V₃O_{0.6}-3 % C hydride releases 6.5 wt% of hydrogen in <3 min. The curves of hydrogen desorption from ternary composites at temperatures of 300, 325, and 350 °C under an initial pressure of hydrogen in a closed volume of 0.02 MPa are shown in SI part S2, Fig. S2-2. The obtained results indicate that the kinetics of the desorption reaction in temperature dependent.

The results of the phase analysis of the samples after the first desorption of hydrogen from hydride composites at 350 °C are shown in Table 4. The X-ray diffraction profiles of the Mg-10%Zr₃V₃O_{0.6}-3%C composite after hydrogen desorption and rehydrogenation at 200 °C under 2 MPa H₂ are shown in SI part S2, Fig. S2-3. It should be noted that after the first desorption of hydrogen from the hydride composite, the magnesium metal phase transforms into a microcrystalline state while the η -phase remains nanocrystalline. The reason for this change is the sintering of magnesium at elevated temperatures ($\geq 300^\circ\text{C}$). No signs of additional phases, which would indicate a chemical interaction between Mg and Zr₃V₃O_{0.6} (or between the corresponding hydrides) in the process of reactive milling in hydrogen (or in subsequent desorption-absorption cycles), were observed in the X-ray patterns.

To estimate the activation energy (E_a) of hydrogen desorption, a series of TDS spectra were measured at different heating rates of 0.5, 1, 2, and 5 °C/min. The obtained data were further processed by Kissinger method [45,63] (Fig. 6). The calculated Kissinger dependence is shown in Fig. 7. The calculated activation energy of hydrogen release is 58 kJ/mol H₂ and 83 kJ/mol H₂ for Mg–10 % Zr₃V₃O_{0.6}-3%C and Mg–10 % Zr₃V₃O_{0.6}, respectively.

The outstanding effects of the oxygen-stabilized compounds η -Ti₄Fe₂O_x and η -Zr₄Fe₂O_x on the kinetics of hydrogenation and dehydrogenation reactions were demonstrated earlier [45,72]. The comparison shows that the activation energy (E_a) of hydrogen desorption for the MgH₂-Ti₄Fe₂O_{0.5}H_x composite (67 kJ/mol) is very close to the one observed in this work, E_a for MgH₂-Zr₃V₃O_{0.6}H_{~10}-3%C (58 kJ/mol), and is much lower in comparison with 146 kJ/mol for a pure MgH₂. First of all, the catalytic effect can be explained by the influence of Zr₃V₃O_x or Ti/Zr₄Fe₂O_x particles that are very effective sources of atomic H and convenient diffusion pathways from/to the Mg/MgH₂ interface during the hydrogenation and dehydrogenation process. Similar properties of

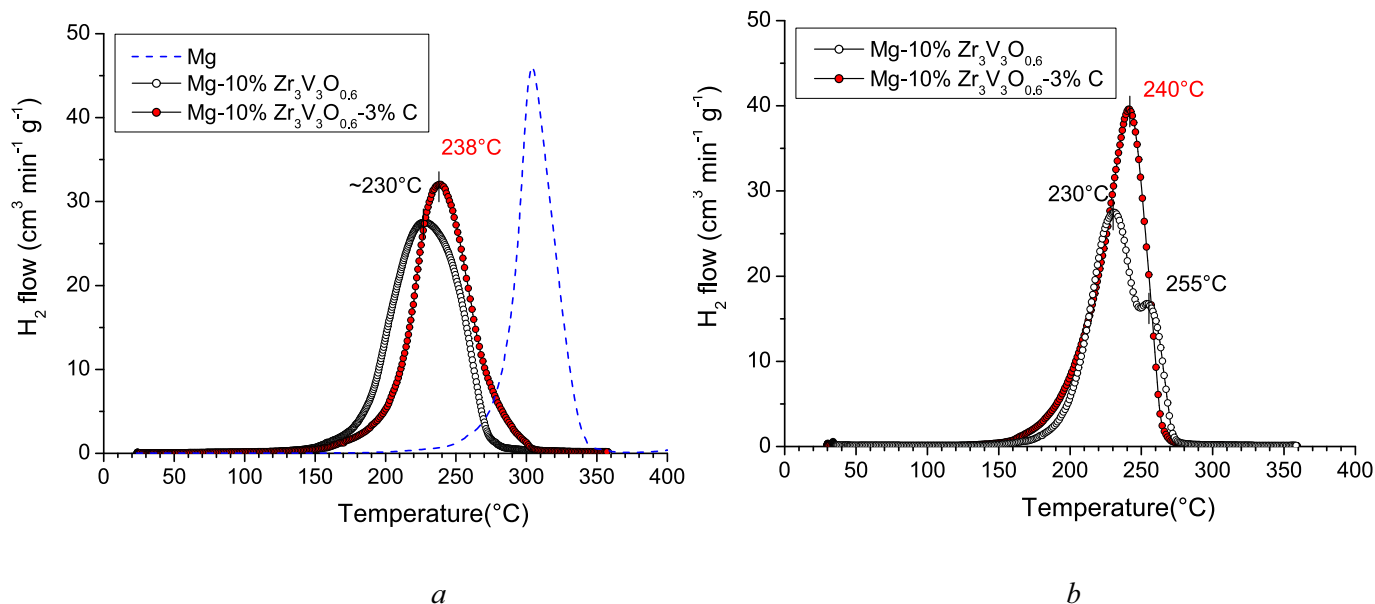


Fig. 5. Spectra of vacuum thermodesorption (TDS) from the hydride composites after mechanochemical milling (a) and after rehydrogenation at 200 °C under 2 MPa H₂ (b). The sample heating rate is 2 °C/min.

Table 4

Phase-structural characteristics of the materials after hydrogen desorption according to the results of refinement by the Rietveld method.

Material	Phase	Space group	Lattice parameters, Å	Content, wt%	The size of the crystallites (D_V), nm; microstress (ϵ), %
Mg-10%Zr ₃ V ₃ O _{0.6}	Mg	$P6_3/mmc$	$a = 3.2091(1)$ $c = 5.2107(2)$	85.9(1)	$D_V = 89(5)$ $\epsilon = 0.06(1)$
	Zr ₃ V ₃ O _{0.6} H ₋₅	$Fd\bar{3}m$	$a = 12.554(3)$	10.1(1)	-
	α -Fe	$Im\bar{3}m$	$a = 2.878(3)$	0.7(1)	-
	MgO	$Fm\bar{3}m$	$a = 4.210(3)$	3.3(2)	-
Mg-10%Zr ₃ V ₃ O _{0.6} -3%C	Mg	$P6_3/mmc$	$a = 3.2094(1)$ $c = 5.2101(2)$	86.8(1)	$D_V = 98(12)$ $\epsilon = 0.11(2)$
	Zr ₃ V ₃ O _{0.6} H ₋₅	$Fd\bar{3}m$	$a = 12.647(5)$	8.4(2)	-
	α -Fe	$Im\bar{3}m$	$a = 2.880(3)$	1.0(1)	-
	MgO	$Fm\bar{3}m$	$a = 4.211(4)$	3.8(4)	-

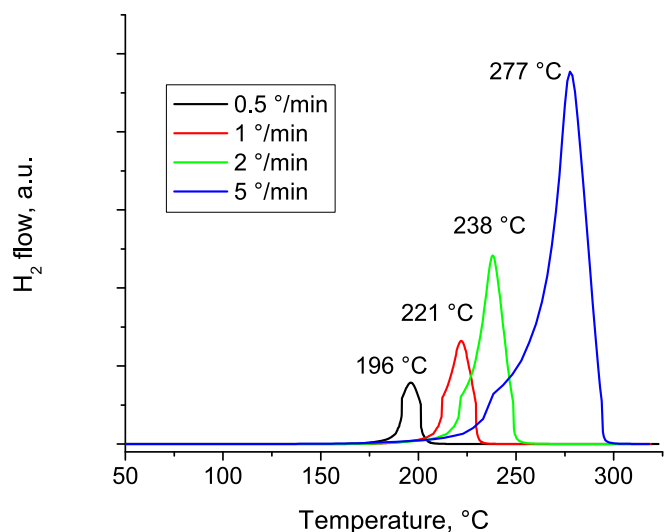


Fig. 6. TDS for the MgH₂-Zr₃V₃O_{0.6}H_x-C composite at different heating rates.

Mg-based composites containing O-stabilized Ti/Zr-based intermetallics as effective additives, indicate that we are dealing with the same phenomenon, which is determined by the chemical nature of these

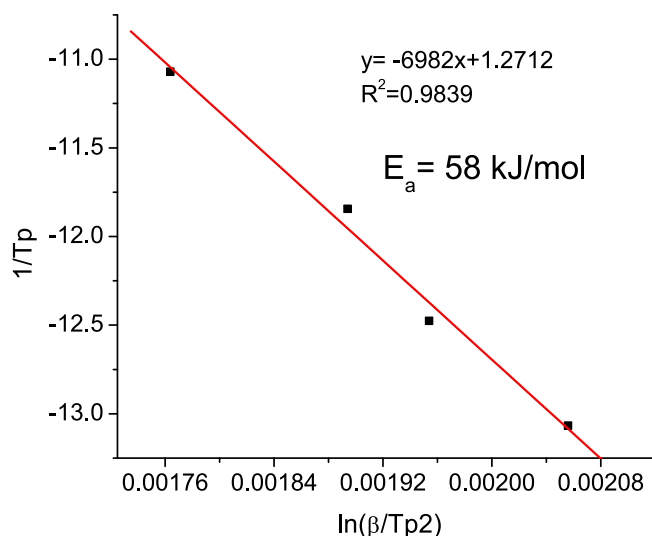


Fig. 7. The fit of the experimental data to derive the activation energy of hydrogen desorption from the MgH₂-Zr₃V₃O_{0.6}H_x-C composite.

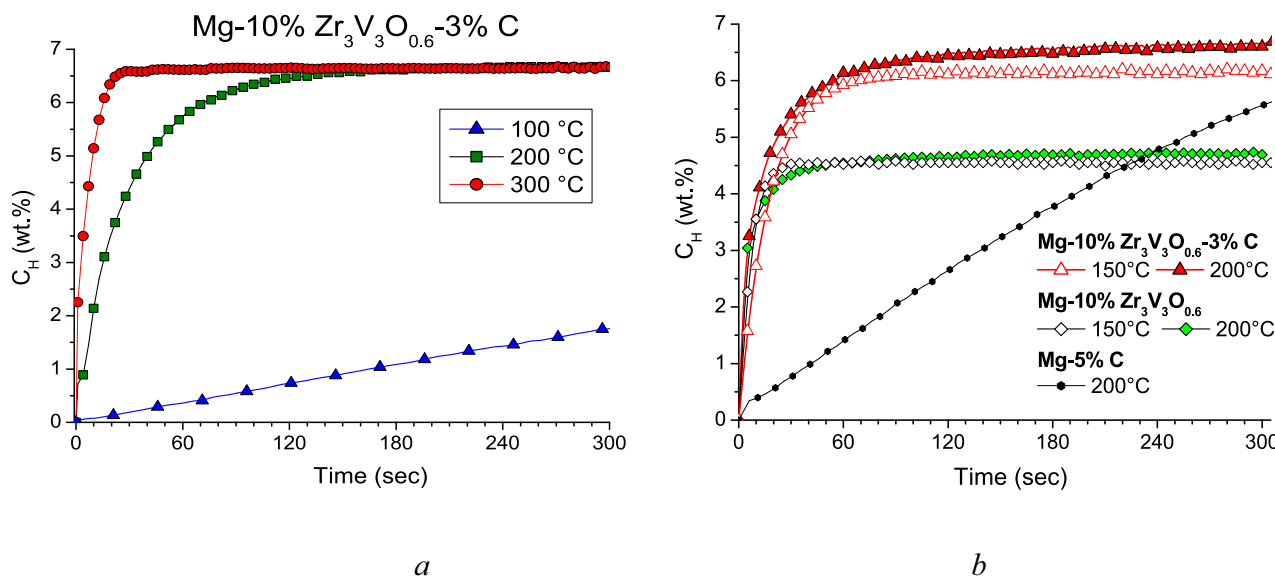


Fig. 8. Curves of hydrogen absorption by Mg-10%Zr₃V₃O_{0.6} and Mg-10%Zr₃V₃O_{0.6}-3%C composites under hydrogen pressure of 2 MPa.

compounds. By analyzing the advantages of the O-stabilized compounds as catalytic additives, we can state that they are characterized by a more efficient activation as compared to TiFe [73] and show much lower hydrogenation/dehydrogenation temperatures than that for Ti/TiH₂ or Zr/ZrH₂. Zr₃V₃O_{0.6} and Ti/Zr₄Fe₂O_x suboxides provide an additional H storage capacity as compared to the inert to hydrogen metals or metal oxides.

After a completion of hydrogen desorption from the hydride composites, they were rehydrogenated under an H₂ pressure of 2 MPa at temperatures from 20 to 350 °C. The ternary composites slowly absorbed hydrogen even at room temperature, but required several hours to form saturated hydrides. The rate of hydrogen absorption increased significantly with increasing temperature. Hydrogen absorption curves at temperatures of 100, 200, and 300 °C are shown in Fig. 8a. At 100 °C, the Mg-10%Zr₃V₃O_{0.6}-3%C composite reaches a capacity of 6 wt% in ~60 min after the start of hydrogenation, while at 200 °C it occurs in just 60 s. At a temperature of 300 °C, hydrogen absorption is very fast, namely a full saturation by hydrogen (6.5 wt% H) occurs in 20 s.

To study the influence of carbon on the properties of composites, samples of Mg-10%Zr₃V₃O_{0.6} and Mg-10%Zr₃V₃O_{0.6}-3%C composites after H₂ desorption into a dynamic vacuum (10⁻³ Pa) at 350 °C were rehydrogenated under the same conditions. The curves of hydrogen absorption by these composites at temperatures of 150 and 200 °C are shown in Fig. 8b. At these temperatures, both composites are characterized by a very high rate of hydrogen absorption. However, in the material that does not contain carbon, absorption practically stops when hydrogen sorption capacity of 4.3–4.5 wt% is reached (which corresponds to the conversion of Mg into MgH₂ by 65–70 %). This is probably caused by the formation of a continuous hydride layer at the surface of the magnesium particle. Since in the case of a material that does not contain carbon, its main part (77.1 wt%) consists of the particles with a size >3 μm (see Table 3), we can assume that at a certain thickness of the hydride layer (<3 μm) further hydrogen diffusion inside of the particles is hindered and the magnesium metal core remains unhydrogenated.

The Mg-10%Zr₃V₃O_{0.6}-3%C composite under similar experimental conditions is almost completely saturated with hydrogen within 1 min, and its capacity is ~6.5 wt%, which practically corresponds to the complete transformation of magnesium into magnesium hydride. The explanation for this can again be in a size distribution of the formed composite (see Table 3), from which it follows that in the case of the C-containing composite, the main part of the sample consists of the particles with a size of 1–3 μm (81.1 wt%).

Therefore, the addition of graphite made it possible to obtain a composite with a significantly smaller particle size further to a slight decrease in the size of the crystallites (see Tables 2–3). This significant difference in particle size distribution probably explains the difference in the amount of absorbed hydrogen at 200 °C for the composites with and without carbon. We note that the fast kinetics of hydrogenation of Mg–Zr₃V₃O_{0.6}–C ternary composites is exclusively caused by the catalytic effect of Zr₃V₃O_{0.6}. The rate of hydrogen absorption during the rehydrogenation of the Mg–C composites is an order of magnitude lower than that for Mg–Zr₃V₃O_{0.6}–C. For comparison, Fig. 8 shows the curve of hydrogen absorption by the Mg-5%C composite at a temperature of 200 °C under a pressure of 2 MPa. This material reaches a full saturation by hydrogen (7.2 wt% H) in 15 min, after the start of the hydrogenation.

Another advantage of use of composites with graphite is that its addition also increases the cyclic stability of the materials during hydrogen absorption/desorption [39,45,67]. Composites Mg–Zr₃V₃O_{0.6}–C during five cycles (see SI part S2, Fig. S2-1) and Mg–Ti₄Fe₂O_{0.3}–C during 20 cycles [45] retained the initial capacity, while for Mg–Ti₄Fe₂O_{0.5} a significant decrease in capacity was observed already in the 7th cycle. The reason for these improvements in stability for the C-containing hydride composites is probably due to the fact that graphite is uniformly distributed on the surface of the particles (SI, part S3) and prevents agglomeration and sintering of the particles during hydrogen desorption, which occurs at elevated temperature.

Thus, in this and earlier work [45], we have shown that the mechanochemical modification of magnesium by oxygen-stabilized intermetallic compounds based on titanium and zirconium leads to a significant decrease in the hydrogenation temperature of magnesium and improvement of absorption-desorption kinetics, while the addition of carbon increases the extent of Mg → MgH₂ conversion and improves the cyclic stability of the composite during multiple cycles of hydrogen absorption-desorption.

3.4. Generation of hydrogen by hydrolysis

Hydrogen generation systems based on use of the hydrolysis process are required for the operation of the fuel cells in light mobile energy supply devices [74,75]. The method of hydrolysis of materials based on magnesium hydride is one of the most acceptable for the “green” hydrogen production for portable energy supply [76,77]. Ball milling can effectively increase the rate of hydrogen release and the reaction yield during the hydrolysis. The influence of the milling conditions and

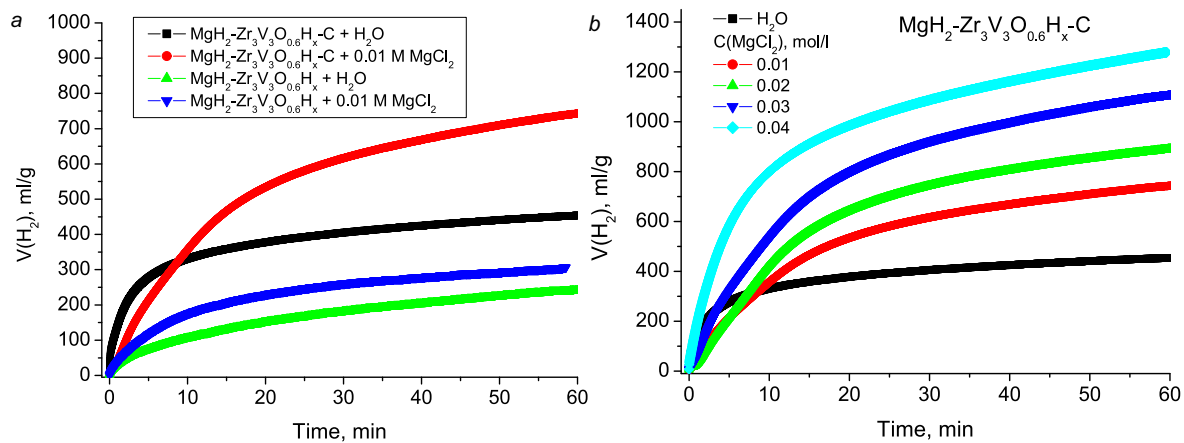


Fig. 9. Curves of hydrogen release during the hydrolysis reaction for the composite materials: a - $\text{MgH}_2\text{-Zr}_3\text{V}_3\text{O}_{0.6}\text{H}_x$ and $\text{MgH}_2\text{-Zr}_3\text{V}_3\text{O}_{0.6}\text{H}_x\text{-C}$ in pure water and 0.01 MgCl_2 solution, b - $\text{MgH}_2\text{-Zr}_3\text{V}_3\text{O}_{0.6}\text{H}_x\text{-C}$ in 0...0.04 MgCl_2 solutions.

the state of dispersion of MgH_2 on the hydrolysis reaction in pure water was studied in [78–83]. In all cases, it was noted that hydrogen yield was low, and was improved after the milling. This can be explained by the fact that the milling increases the specific surface area of the materials. A significant additional effect is achieved when graphite is added during mechanical milling of MgH_2 . MgH_2 -graphite composites release up to 970–1280 ml of hydrogen per gram of the composite in 40 min of hydrolysis without changes in the acidity of the solution [81]. Therefore, mechanical milling of MgH_2 -graphite mixtures is a promising approach to obtaining highly efficient materials for autonomous hydrogen generators. The additional use of the $\text{Zr}_3\text{V}_3\text{O}_{0.6}$ catalyst makes it possible to reduce the magnesium hydride synthesis time by 3–4 times. Therefore, the synthesized materials were tested as sources of hydrogen production by the hydrolysis method, and the effect of the used catalysts on the total hydrogen yield was established. The hydrolysis of the binary synthesized composite $\text{MgH}_2\text{-Zr}_3\text{V}_3\text{O}_{0.6}\text{H}_{\sim 10}$ demonstrated a much lower conversion extent than that for ternary composite $\text{MgH}_2\text{-Zr}_3\text{V}_3\text{O}_{0.6}\text{H}_{\sim 10}\text{-C}$ in pure water and in 0.01 M MgCl_2 water solution (Fig. 9a). The increased quantity of the released hydrogen in 0.01 M MgCl_2 solutions motivated additional studies of the hydrogen evaluation from the $\text{MgH}_2\text{-Zr}_3\text{V}_3\text{O}_{0.6}\text{H}_{\sim 10}\text{-C}$ composite in water solutions with different MgCl_2 content (Fig. 9b). They demonstrated 1278 ml/g released in 60 min or 1364 ml/g in 120 min (the conversion degree is ~ 80 and 85% , respectively) from the ternary composite interacting with 0.04 M MgCl_2 solution. The main reason of such enhancement for C-containing ternary composite may be related to the substantial decrease of the particle size. The role of $\text{Zr}_3\text{V}_3\text{O}_{0.6}$ additives in hydrolysis reaction will be clarified in further studies. At this moment we can state that the $\text{MgH}_2\text{-Zr}_3\text{V}_3\text{O}_{0.6}\text{H}_{\sim 10}\text{-C}$ composite, which was synthesized as the effective hydrogen storage material, can be used as effective material for both hydrogen storage and hydrogen generation by hydrolysis process.

4. Conclusions

The catalytic effect of additions of $\eta\text{-Zr}_3\text{V}_3\text{O}_{0.6}$ suboxide and the same intermetallic and graphite on the hydrogen absorption-desorption properties of MgH_2 has been investigated for the first time. It was shown that these composites are able to absorb ~ 6.5 wt% of hydrogen in a few minutes under reactive ball milling conditions in hydrogen gas. It was found that the addition of $\text{Zr}_3\text{V}_3\text{O}_{0.6}$ and $\text{Zr}_3\text{V}_3\text{O}_{0.6} + \text{C}$ catalysts not only increases the rates of hydrogen absorption and release, but also lowers the activation energy and the temperature of hydrogen release. For the sample containing 10 wt% of the suboxide and 3 wt% of graphite, the activation energy of hydrogen desorption and temperature of release were determined as 58 kJ/mol and 196 °C, respectively. This E_a value is slightly lower than that for dehydrogenation of the $\text{Mg} + 1$

mol% $\text{Ti}_4\text{Fe}_2\text{O}_{0.5}$ composite (67 kJ/mol H_2) and is much lower in comparison with 146 kJ/mol for the pure MgH_2 . Thus, the values of dehydrogenation activation energies of the studied Mg-based composites with Ti/Zr-based suboxides as catalytic additives are among the lowest described in the reference data.

The improvement of the kinetics and increase of hydrogen capacity at operating temperatures of 150–200 °C are particularly characteristic for the composites with suboxide and graphite additions. It was shown that the reason for this improvement is the difference in the morphology of the synthesized samples, namely the introduction of graphite during the milling leads to a better dispergation of the material (the fraction with a particle size of 1–3 μm is >80 wt%).

Absorption-desorption tests demonstrated the stable capacity of the synthesized $\text{Mg-Zr}_3\text{V}_3\text{O}_{0.6}\text{-C}$ composite (~ 6.5 wt% during 5 first cycles). This behavior is very similar to that of $\text{Mg-Ti}_4\text{Fe}_2\text{O}_x\text{-C}$ material for 20 cycles. Both these composites demonstrated the substantial cycling increase, because of the graphite additions. The possible reason of such an important feature could be a decreased ability of C-containing composites to agglomeration during the heating.

The hydrogen generation in the hydrolysis reaction was studied as well. The amount of hydrogen released from the hydride $\text{Mg-Zr}_3\text{V}_3\text{O}_{0.6}\text{-C}$ composite in the hydrolysis reaction reaches 1364 ml/g for 120 min (the conversion degree is $\sim 85\%$) when using 0.04 M MgCl_2 solutions. We conclude that the $\text{Mg-Zr}_3\text{V}_3\text{O}_{0.6}\text{-C}$ composite can be used as the effective hydrogen storage material as well as the material for hydrogen generation in the hydrolysis process.

CRediT authorship contribution statement

Ihor Zavaliiy: Conceptualization, Supervision, Investigation, Writing – review & editing, Project administration, Funding acquisition. **Vasyl Berezovets:** Investigation, Formal analysis, Visualization, Writing – original draft, Writing – review & editing. **Roman Denys:** Investigation, Formal analysis, Visualization, Writing – original draft. **Oleksandr Kononiuk:** Investigation, Formal analysis, Visualization, Writing – original draft. **Volodymyr Yartys:** Conceptualization, Supervision, Formal analysis, Writing – review & editing.

Declaration of competing interest

The authors declare that they have no known competing financial interests or personal relationships that could have appeared to influence the work reported in this paper.

Data availability

No data was used for the research described in the article.

Acknowledgements

The work received a support from the National Research Foundation of Ukraine, project No. 2020.02/0301 “Development of new functional materials for the needs of hydrogen energy”.

Appendix A. Supplementary data

Supplementary data to this article can be found online at <https://doi.org/10.1016/j.est.2023.107245>.

References

- [1] Y. Sun, C. Shen, Q. Lai, W. Liu, D.W. Wang, K.F. Aguey-Zinsou, Tailoring magnesium based materials for hydrogen storage through synthesis: current state of the art, *Energy Storage Mater.* 10 (2018) 168–198, <https://doi.org/10.1016/j.ensm.2017.01.010>.
- [2] B. Sakintuna, F. Lamari-Darkrim, M. Hirscher, Metal hydride materials for solid hydrogen storage: a review, *Int. J. Hydrog. Energy* 32 (2007) 1121–1140, <https://doi.org/10.1016/j.ijhydene.2006.11.022>.
- [3] V.A. Yartys, M.V. Lototsky, E. Akiba, R. Albert, V.E. Antonov, J.R. Ares, M. Baricco, N. Bourgeois, C.E. Buckley, J.M. Bellosta von Colbe, J.-C. Crivello, F. Cuevas, R.V. Denys, M. Dornheim, M. Felderhoff, D.M. Grant, B.C. Hauback, T. D. Humphries, I. Jacob, T.R. Jensen, P.E. de Jongh, J.-M. Joubert, M. A. Kuzovnikova, M. Latroche, M. Paskevicius, L. Pasquini, L. Popilevsky, V. M. Skripnyuk, E. Rabkin, M.V. Sofianos, A. Stuart, G. Walker, H. Wang, C.J. Webb, M. Zhu, Magnesium based materials for hydrogen based energy storage: past, present and future, *Int. J. Hydrog. Energy* 44 (2019) 7809–7859, <https://doi.org/10.1016/j.ijhydene.2018.12.212>.
- [4] J.F. Fernandez, C.R. Sanchez, Rate determining step in the absorption and desorption of hydrogen by magnesium, *J. Alloys Compd.* 340 (2002) 189–198, [https://doi.org/10.1016/S0925-8388\(02\)00120-2](https://doi.org/10.1016/S0925-8388(02)00120-2).
- [5] Norkov, A. Houmuller, P. Johansson, B.I. Lundqvist, Adsorption and dissociation of H₂ on Mg surfaces, *Phys. Rev. Lett.* 46 (1981) 257–261, <https://doi.org/10.1103/PhysRevLett.46.257>.
- [6] A. Baran, M. Polanski, Magnesium-based materials for hydrogen storage—a scope review, *Materials* 13 (3993) (2020) 1–55, <https://doi.org/10.3390/ma13183993>.
- [7] C.J. Webb, A review of catalyst-enhanced magnesium hydride as a hydrogen storage material, *J. Phys. Chem. Solids* 85 (2015) 96–106, <https://doi.org/10.1016/j.jpcs.2014.06.014>.
- [8] L. Ouyang, F. Liu, H. Wang, J. Liu, X.S. Yang, L. Sun, M. Zhu, Magnesium-based hydrogen storage compounds: a review, *J. Alloys Compd.* 832 (2020), 154865, <https://doi.org/10.1016/j.jallcom.2020.154865>.
- [9] X. Xie, M. Chen, M. Hu, B. Wang, R. Yu, T. Liu, Recent advances in magnesium-based hydrogen storage materials with multiple catalysts, *Int. J. Hydrog. Energy* 44 (2019) 10694–10712, <https://doi.org/10.1016/j.ijhydene.2019.02.237>.
- [10] M. Polanski, J. Bystrycki, Comparative studies of the influence of different nano-sized metal oxides on the hydrogen sorption properties of magnesium hydride, *J. Alloys Compd.* 486 (2009) 697–701, <https://doi.org/10.1016/j.jallcom.2009.07.042>.
- [11] I.Yu. Zavaliy, V.V. Berezovets, R.V. Denys, Nanocomposites based on magnesium for hydrogen storage: achievements and prospects (A survey), *Mater. Sci.* 54 (2019) 611–626, <https://doi.org/10.1007/s11003-019-00226-x>.
- [12] A. Zaluska, L. Zaluski, J.O. Strom-Olsen, Nanocrystalline magnesium for hydrogen storage, *J. Alloys Compd.* 288 (1999) 217–225, [https://doi.org/10.1016/S0925-8388\(99\)00073-0](https://doi.org/10.1016/S0925-8388(99)00073-0).
- [13] J.-C. Crivello, B. Dam, R.V. Denys, M. Dornheim, D.M. Grant, J. Huot, T.R. Jensen, P. de Jongh, M. Latroche, C. Milanese, D. Milcius, G.S. Walker, C.J. Webb, C. Zlotea, V.A. Yartys, Review of magnesium hydride-based materials: development and optimization, *Appl. Phys. A Mater. Sci. Process.* 122 (2016) 97, <https://doi.org/10.1007/s00339-016-9602-0>.
- [14] Y.V. Verbovytsky, V.V. Berezovets, A.R. Kytysya, I.Y. Zavaliy, V.A. Yartys, Hydrogen generation by the hydrolysis of MgH₂, *Mater. Sci.* 56 (2020) 1–14, <https://doi.org/10.1007/s11003-020-00390-5>.
- [15] M.V. Lototsky, R.V. Denys, V.A. Yartys, Combustion-type hydrogenation of nanostructured Mg-based composites for hydrogen storage, *Int. J. Energy Res.* 33 (2009) 1114–1125, <https://doi.org/10.1002/er.1604>.
- [16] G. Liang, J. Huot, S. Boily, A. Van Neste, R. Schulz, Catalytic effect of transition metals on hydrogen sorption in nanocrystalline ball milled MgH₂-Tm (Tm=Ti, V, Mn, Fe and Ni) systems, *J. Alloys Compd.* 292 (1999) 247–252, [https://doi.org/10.1016/S0925-8388\(99\)00442-9](https://doi.org/10.1016/S0925-8388(99)00442-9).
- [17] N. Hanada, T. Ichikawa, H. Fujii, Catalytic effect of nanoparticle 3d-transition metals on hydrogen storage properties in magnesium hydride MgH₂ prepared by mechanical milling, *J. Phys. Chem. B* 109 (2005) 7188–7194, <https://doi.org/10.1021/jp044576c>.
- [18] T. Sadhasivam, H.T. Kim, S. Jung, S.H. Roh, J.H. Park, H.Y. Jung, Dimensional effects of nanostructured Mg/MgH₂ for hydrogen storage applications: a review, *Ren. Sust. Energy Rev.* 72 (2017) 523–534, <https://doi.org/10.1016/j.rser.2017.01.107>.
- [19] M.P. Pitt, M. Paskevicius, C.J. Webb, D.A. Sheppard, C.E. Buckley, E.MacA. Gray, The synthesis of nanoscopic Ti based alloys and their effects on the MgH₂ system compared with the MgH₂+0.01Nb₂O₅ benchmark, *Int. J. Hydrog. Energy* 37 (2012) 4227–4237, <https://doi.org/10.1016/j.ijhydene.2011.11.114>.
- [20] H. Gasan, O.N. Celik, N. Aydinbeyli, Y.M. Yaman, Effect of V, Nb, Ti and graphite additions on the hydrogen desorption temperature of magnesium hydride, *Int. J. Hydrog. Energy* 37 (2012) 1912–1918, <https://doi.org/10.1016/j.ijhydene.2011.05.086>.
- [21] W. Oelerich, T. Klassen, R. Bormann, Metal oxides as catalysts for improved hydrogen sorption in nanocrystalline Mg-based materials, *J. Alloys Compd.* 315 (2001) 237–242, [https://doi.org/10.1016/S0925-8388\(00\)01284-6](https://doi.org/10.1016/S0925-8388(00)01284-6).
- [22] G. Barkhordarian, T. Klassen, R. Bormann, Effect of Nb₂O₅ content on hydrogen reaction kinetics of Mg, *J. Alloys Compd.* 364 (2004) 242–246, [https://doi.org/10.1016/S0925-8388\(03\)00530-9](https://doi.org/10.1016/S0925-8388(03)00530-9).
- [23] Y. Kojima, Y. Kawai, T. Haga, Magnesium-based nanocomposite materials for hydrogen storage, *J. Alloys Compd.* 424 (2006) 294–298, <https://doi.org/10.1016/j.jallcom.2005.11.088>.
- [24] M. Lototsky, M.W. Davids, J.M. Sibanyoni, J. Goh, B.G. Pollet, Magnesium-based hydrogen storage nanomaterials prepared by high energy reactive ball milling in hydrogen at the presence of mixed titanium–iron oxide, *J. Alloys Compd.* 645 (2015) S454–S459, <https://doi.org/10.1016/j.jallcom.2014.12.084>.
- [25] N. Hanada, T. Ichikawa, S. Isobe, T. Nakagawa, K. Tokoyoda, T. Honma, H. Fujii, Y. Kojima, X-ray absorption spectroscopic study on valence state and local atomic structure of transition metal oxides doped in MgH₂, *J. Phys. Chem. C* 113 (2009) 13450–13455, <https://doi.org/10.1021/jp901859f>.
- [26] R.R. Shahi, A.P. Tiwari, M.A. Shaz, O.N. Srivastava, Studies on de/rehydrogenation characteristics of nanocrystalline MgH₂ co-catalyzed with Ti, Fe and Ni, *Int. J. Hydrog. Energy* 38 (2013) 2778–2784, <https://doi.org/10.1016/j.ijhydene.2012.11.073>.
- [27] M. Calizzi, D. Chericoni, L.H. Jepsen, T.R. Jensen, L. Pasquini, Mg-Ti nanoparticles with superior kinetics for hydrogen storage, *Int. J. Hydrog. Energy* 41 (2016) 14447–14454, <https://doi.org/10.1016/j.ijhydene.2016.03.071>.
- [28] B.S. Amirkhiz, B. Zahiri, P. Kalisvaart, D. Mitlin, Synergy of elemental Fe and Ti promoting low temperature hydrogen sorption cycling of magnesium, *Int. J. Hydrog. Energy* 36 (2011) 6711–6722, <https://doi.org/10.1016/j.ijhydene.2011.02.141>.
- [29] R.A. Varin, Z. Zaranski, T. Czujko, M. Polanski, Z.S. Wronski, The composites of magnesium hydride and iron-titanium intermetallic, *Int. J. Hydrog. Energy* 36 (2011) 1177–1183, <https://doi.org/10.1016/j.ijhydene.2010.06.092>.
- [30] B.P. Tarasov, A.A. Arbuzov, S.A. Mozzhuhin, A.A. Volodin, P.V. Fursikov, M. V. Lototsky, V.A. Yartys, Hydrogen storage behavior of magnesium catalyzed by nickel-graphene nanocomposites, *Int. J. Hydrog. Energy* 44 (2019) 29212–29223, <https://doi.org/10.1016/j.ijhydene.2019.02.033>.
- [31] M. Lototsky, J. Goh, M.W. Davids, V. Linkov, L. Khotseng, B. Ntsendwana, R. Denys, V.A. Yartys, Nanostructured hydrogen storage materials prepared by high-energy reactive ball milling of magnesium and ferromagnesium, *Int. J. Hydrog. Energy* 44 (2019) 6687–6701, <https://doi.org/10.1016/j.ijhydene.2019.01.135>.
- [32] M. Chen, X. Xiao, M. Zhang, J. Zheng, M. Liu, X. Wang, L. Jiang, L. Chen, Highly dispersed metal nanoparticles on TiO₂ acted as nano redox reactor and its synergistic catalysis on the hydrogen storage properties of magnesium hydride, *Int. J. Hydrog. Energy* 44 (2019) 15100–15109, <https://doi.org/10.1016/j.ijhydene.2019.04.047>.
- [33] M.Y. Song, S.N. Kwon, H.R. Park, J.L. Bobet, Improvement of hydriding and dehydriding rates of Mg via addition of transition elements Ni, Fe, and Ti, *Int. J. Hydrog. Energy* 36 (2011) 12932–12938, <https://doi.org/10.1016/j.ijhydene.2011.07.054>.
- [34] H.Y. Sohn, S. Emami, Kinetics of dehydrogenation of the Mg–Ti–H hydrogen storage system, *Int. J. Hydrog. Energy* 36 (2011) 8344–8350, <https://doi.org/10.1016/j.ijhydene.2011.03.167>.
- [35] L. Zhang, X. Lu, L. Ji, N. Yan, Z. Sun, X. Zhu, Catalytic effect of facile synthesized TiH_{1.971} nanoparticles on the hydrogen storage properties of MgH₂, *Nanomaterials* 9 (2019) 1370, <https://doi.org/10.3390/nano9101370>.
- [36] T. Liu, C.G. Chen, F. Wang, X.G. Li, Enhanced hydrogen storage properties of magnesium by the synergistic catalytic effect of TiH_{1.971} and TiH_{1.5} nanoparticles at room temperature, *J. Power Sources* 267 (2014) 69–77, <https://doi.org/10.1016/j.jpowsour.2014.05.066>.
- [37] N. Patelli, M. Calizzi, A. Migliori, V. Morandi, L. Pasquini, Hydrogen desorption below 150 °C in MgH₂-TiH₂ composite nanoparticles: equilibrium and kinetic properties, *J. Phys. Chem. C* 121 (2017) 11166–11177, <https://doi.org/10.1021/acs.jpcc.7b03169>.
- [38] J. Lu, Y.J. Choi, Z.Z. Fang, H.Y. Sohn, E. Ronnebro, Hydrogen storage properties of nanosized MgH₂-0.1TiH₂ prepared by ultrahigh-energy-high pressure milling, *J. Am. Chem. Soc.* 131 (2009) 15843–15852, <https://doi.org/10.1021/ja906340u>.
- [39] M.V. Lototsky, R.V. Denys, V.A. Yartys, J. Eriksen, J. Goh, S. Nyallang Nyamsi, C. Sita, F. Cummings, An outstanding effect of graphite in nano-MgH₂-TiH₂ on hydrogen storage performance, *J. Mater. Chem. A* 6 (2018) 10740–10754, <https://doi.org/10.1039/C8TA02969E>.
- [40] M. Chen, Y. Wang, X. Xiao, Y. Lu, M. Zhang, J. Zheng, L. Chen, Highly efficient ZrH₂ nanocatalyst for the superior hydrogenation kinetics of magnesium hydride under moderate conditions: investigation and mechanistic insights, *Appl. Surf. Sci.* 541 (2021), 148375, <https://doi.org/10.1016/j.apsusc.2020.148375>.
- [41] L. Zhang, Z. Sun, Z. Cai, N. Yan, X. Lu, X. Zhu, L. Chen, Enhanced hydrogen storage properties of MgH₂ by the synergistic catalysis of Zr_{0.4}Ti_{0.6}Co nanosheets and

- carbon nanotubes, *Appl. Surf. Sci.* 504 (2020), 144465, <https://doi.org/10.1016/j.apsusc.2019.144465>.
- [42] L. Zhang, Z. Cai, Z. Yao, L. Ji, S. Ze, N. Yan, B. Zhang, B. Xiao, J. Du, X. Zhu, L. Chen, A striking catalytic effect of facile synthesized ZrMn₂ nanoparticles on the de/rehydrogenation properties of MgH₂, *J. Mater. Chem. A* 7 (2019) 5626–5634, <https://doi.org/10.1039/c9ta00120d>.
- [43] R.R. Shahi, A. Bhatnagar, S.K. Pandey, V. Shukla, T.P. Yadav, M.A. Shaz, O. N. Srivastava, MgH₂-ZrFe₂H_x nanocomposites for improved hydrogen storage characteristics of MgH₂, *Int. J. Hydrog. Energy* 40 (2015) 11506–11513, <https://doi.org/10.1016/j.ijhydene.2015.03.162>.
- [44] C.S. Zhou, Z.G.Z. Fang, R.C. Bowman, Stability of catalyzed magnesium hydride nanocrystalline during hydrogen cycling. Part I: Kinetic Analysis, *J. Phys. Chem. C* 119 (2015) 22261–22271, <https://doi.org/10.1021/acs.jpcc.5b06190>.
- [45] V.V. Berezovets, R.V. Denys, I.Yu. Zavaliiy, Y.V. Kosarchyn, Effect of Ti-based nanosized additives on the hydrogen storage properties of MgH₂, *Int. J. Hydrog. Energy* 47 (2022) 7289–7298, <https://doi.org/10.1016/j.ijhydene.2021.03.019>.
- [46] I.Yu. Zavaliiy, R.V. Denys, I.V. Koval'chuk, A.B. Riabov, R.G. Delaplane, Hydrogenation of Ti_{4-x}Zr_xFe₂O_y alloys and crystal structure analysis of their deuterides, *Chem. Met. Alloys* 2 (2009) 59–67.
- [47] I.Yu. Zavaliiy, Effect of oxygen content on hydrogen storage capacity of Zr-based η-phases, *J. Alloys Compd.* 291 (1999) 102–109, [https://doi.org/10.1016/S0925-8388\(99\)00187-5](https://doi.org/10.1016/S0925-8388(99)00187-5).
- [48] I.Yu. Zavaliiy, W.B. Yelon, P.Y. Zavalij, I.V. Saldan, V.K. Pecharsky, The crystal structure of the oxygen-stabilized η-phase Zr₃V₃O₇D_{9.6}, *J. Alloys Compd.* 309 (2000) 75–82, [https://doi.org/10.1016/S0925-8388\(00\)00899-9](https://doi.org/10.1016/S0925-8388(00)00899-9).
- [49] S.D. Kuschch, N.S. Kuyunko, R.S. Nazarov, B.P. Tarasov, Hydrogen-generating compositions based on magnesium, *Int. J. Hydrog. Energy* 36 (2011) 1321–1325, <https://doi.org/10.1016/j.ijhydene.2010.06.115>.
- [50] T. Hiraki, S. Hiroi, T. Akashi, N. Okinaka, T. Akiyama, Chemical equilibrium analysis for hydrolysis of magnesium hydride to generate hydrogen, *Int. J. Hydrog. Energy* 37 (2012) 12114–12119, <https://doi.org/10.1016/j.ijhydene.2012.06.012>.
- [51] T. Tayeh, A.S. Awad, M. Nakhil, M. Zakhour, J.F. Silvain, J.L. Bobet, Production of hydrogen from magnesium hydrides hydrolysis, *Int. J. Hydrog. Energy* 39 (2014) 3109–3117, <https://doi.org/10.1016/j.ijhydene.2013.12.082>.
- [52] C.H. Chao, T.C. Jen, Reaction of magnesium hydride with water to produce hydrogen, *Appl. Mech. Mater.* 302 (2013) 151–157, <https://doi.org/10.4028/www.scientific.net/AMM.302.151>.
- [53] M. Tegel, S. Schöne, B. Kieback, L. Röntzsch, An efficient hydrolysis of MgH₂-based materials, *Int. J. Hydrog. Energy* 42 (2017) 2167–2176, <https://doi.org/10.1016/j.ijhydene.2016.09.084>.
- [54] L.G. Sevastyanova, S.N. Klyamkin, B.M. Bulychev, Generation of hydrogen from magnesium hydride oxidation in water in presence of halides, *Int. J. Hydrog. Energy* 45 (2020) 3046–3052, <https://doi.org/10.1016/j.ijhydene.2019.11.226>.
- [55] S. Zhong, C. Wu, J. Li, Y. Chen, Y. Wang, Y. Yan, Effect of cations in chloride solutions on low-temperature hydrolysis performances and mechanisms of Mg–Ca-based hydride, *J. Alloys Compd.* 851 (2021), 156762, <https://doi.org/10.1016/j.jallcom.2020.156762>.
- [56] M. Huang, L. Ouyang, H. Wang, J. Liu, M. Zhu, Hydrogen generation by hydrolysis of MgH₂ and enhanced kinetics performance of ammonium chloride introducing, *Int. J. Hydrog. Energy* 40 (2015) 6145–6150, <https://doi.org/10.1016/j.ijhydene.2015.03.058>.
- [57] V.V. Berezovets, A.R. Kytysya, I.Yu. Zavaliiy, V.A. Yartys, Kinetics and mechanism of hydrolysis of MgH₂ in MgCl₂ solutions, *Int. J. Hydrog. Energy* 46 (2021) 40278–40293, <https://doi.org/10.1016/j.ijhydene.2021.09.249>.
- [58] P. Patnaik, in: *A Comprehensive Guide to the Hazardous Properties of Chemical Substances*, 3rd ed., Wiley, 2008, ISBN 978-0-471-71458-3, pp. 630–642.
- [59] J. Huot, G. Liang, R. Schulz, Magnesium-based nanocomposites chemical hydrides, *J. Alloys Compd.* 353 (2003) L12–L15, [https://doi.org/10.1016/S0925-8388\(02\)01306-3](https://doi.org/10.1016/S0925-8388(02)01306-3).
- [60] X. Zhang, Z. Leng, M. Gao, J. Hu, F. Du, J. Yao, H. Pan, Y. Liu, Enhanced hydrogen storage properties of MgH₂ catalyzed with carbon supported nanocrystalline TiO₂, *J. Power Sources* 398 (2018) 183–192, <https://doi.org/10.1016/j.jpowsour.2018.07.072>.
- [61] S.K. Pandey, A. Bhatnagar, R.R. Shahi, M.S.L. Hudson, M.K. Singh, O.N. Srivastava, Effect of TiO₂ nanoparticles on the hydrogen sorption characteristics of magnesium hydride, *J. Nanosci. Nanotechnol.* 13 (2013) 5493–5499, <https://doi.org/10.1166/jnn.2013.7516>.
- [62] R. Floriano, S. Deledda, B.C. Hauback, D.R. Leiva, W.J. Botta, Iron and niobium based additives in magnesium hydride: Microstructure and hydrogen storage properties, *Int. J. Hydrog. Energy* 42 (2017) 6810–6819, <https://doi.org/10.1016/j.ijhydene.2016.11.117>.
- [63] R.L. Blaine, H.E. Kissinger, Homer Kissinger and the Kissinger equation, *Thermochim. Acta* 540 (2012) 1–6, <https://doi.org/10.1016/j.tca.2012.04.008>.
- [64] A.C. Larson, R.B. von Dreele, General Structure Analysis System (GSAS), Los Alamos National Laboratory Report LAUR 86-748, 2004.
- [65] P.W. Stephens, Phenomenological model of anisotropic peak broadening in powder diffraction, *J. Appl. Crystallogr.* 32 (1999) 281–289, <https://doi.org/10.1107/S0021889898006001>.
- [66] D. Balzar, N. Auderbrand, M.R. Daymond, A. Fitch, A. Hewat, J.I. Langford, A. Le Bail, D. Louër, O. Masson, C.N. McCowan, N.C. Popa, P.W. Stephens, B.H. Toby, Size-strain line-broadening analysis of the ceria round-robin sample, *J. Appl. Crystallogr.* 37 (2004) 911–924, <https://doi.org/10.1107/S0021889804022551>.
- [67] M. Lototsky, J.M. Sibanyoni, R.V. Denys, M. Williams, B.G. Pollet, V.A. Yartys, Magnesium–carbon hydrogen storage hybrid materials produced by reactive ball milling in hydrogen, *Carbon* 57 (2013) 146–160, <https://doi.org/10.1016/j.carbon.2013.01.058>.
- [68] T. Førde, J.P. Maehlen, V.A. Yartys, M.V. Lototsky, H. Uchida, Influence of intrinsic hydrogenation/dehydrogenation kinetics on the dynamic behaviour of metal hydrides: a semi-empirical model and its verification, *Int. J. Hydrog. Energy* 32 (2007) 1041–1049, <https://doi.org/10.1016/j.ijhydene.2006.07.015>.
- [69] J. Huot, G. Liang, S. Boily, A. Van Neste, R. Schulz, Structural study and hydrogen sorption kinetics of ball-milled magnesium hydride, *J. Alloys Compd.* 293–295 (1999) 495–500, [https://doi.org/10.1016/S0925-8388\(99\)00474-0](https://doi.org/10.1016/S0925-8388(99)00474-0).
- [70] R.A. Varin, T. Czujko, Z. Wronski, Particle size, grain size and γ-MgH₂ effects on the desorption properties of nanocrystalline commercial magnesium hydride processed by controlled mechanical milling, *Nanotechnology* 17 (2006) 3856–3865, <https://doi.org/10.1088/0957-4484/17/15/041>.
- [71] R.A. Varin, T. Czujko, C. Chiu, Z. Wronski, Particle size effects on the desorption properties of nanostructured magnesium dihydride (MgH₂) synthesized by controlled reactive mechanical milling (CRMM), *J. Alloys Compd.* 424 (2006) 356–364, <https://doi.org/10.1016/j.jallcom.2005.12.087>.
- [72] V. Berezovets, R. Denis, I. Zavaliiy, V. Paul-Boncour, Powder Metall. Met. Ceram. 53 (5-6) (2014) 335–342, <https://doi.org/10.1007/s11106-014-9621-3>.
- [73] B. Rupp, On the change in physical properties of Ti_{4-x}Fe_{2+x}O_y during hydrogenation I: activation behaviour of ternary oxides Ti_{4-x}Fe_{2+x}O_y and β-Ti, *J. Less-Common Met.* 104/1 (1984) 51–63, [https://doi.org/10.1016/0022-5088\(84\)90435-1](https://doi.org/10.1016/0022-5088(84)90435-1).
- [74] S. Kwon, M.J. Kim, S. Kang, T. Kim, Development of a high-storage-density hydrogen generator using solid-state NaBH₄ as a hydrogen source for unmanned aerial vehicles, *Appl. Energy* 251 (2019), 113331, <https://doi.org/10.1016/j.apenergy.2019.113331>.
- [75] V. Yartys, I. Zavaliiy, V. Berezovets, Y. Pirskyy, F. Manilevich, A. Kytysya, Y. Verbovytsky, Y. Dubov, A. Kutsyi, Hydrogen generator integrated with fuel cell for portable energy supply, *J. Phys. Energy* 5 (2023), 014014, <https://doi.org/10.1088/2515-7655/acab2d>.
- [76] S. Al Bacha, A. Thienpont, M. Zakhour, M. Nakhil, J.-L. Bobet, Clean hydrogen production by the hydrolysis of magnesium-based material: effect of the hydrolysis solution, *J. Clean. Prod.* 282 (2021), 124498, <https://doi.org/10.1016/j.jclepro.2020.124498>.
- [77] S. Al Bacha, S.A. Pighin, G. Urretavizcaya, M. Zakhour, F.J. Castro, M. Nakhil, J.-L. Bobet, Hydrogen generation from ball milled Mg alloy waste by hydrolysis reaction, *J. Power Sources* 479 (2020), 228711, <https://doi.org/10.1016/j.jpowsour.2020.228711>.
- [78] J.-P. Tessier, P. Palau, J. Huot, R. Schulz, D. Guaya, Hydrogen production and crystal structure of ball-milled MgH₂-Ca and MgH₂-CaH₂ mixtures, *J. Alloys Compd.* 376 (2004) 180–185, <https://doi.org/10.1016/j.jallcom.2003.12.013>.
- [79] M.-H. Grosjean, M. Zidoune, L. Roue, Hydrogen production from highly corroding Mg-based materials elaborated by ball milling, *J. Alloys Compd.* 404 (2005) 712–715, <https://doi.org/10.1016/j.jallcom.2004.10.098>.
- [80] M.-H. Grosjean, M. Zidoune, L. Roue, J.-Y. Huot, Hydrogen production via hydrolysis reaction from ball-milled Mg-based materials, *Int. J. Hydrog. Energy* 31 (2006) 109–119, <https://doi.org/10.1016/j.ijhydene.2005.01.001>.
- [81] R.V. Lukashev, N.A. Yakovleva, S.N. Klyamkin, B.P. Tarasov, Effect of mechanical activation on the reaction of magnesium hydride with water, *Russ. J. Inorg. Chem.* 53 (2008) 343–349, <https://doi.org/10.1134/S0036023608030017>.
- [82] L. Ouyang, M. Ma, M. Huang, R. Duan, H. Wang, L. Sun, M. Zhu, Enhanced hydrogen generation properties of MgH₂-based hydrides by breaking the magnesium hydroxide passivation layer, *Energies* 8 (2015) 4237–4252, <https://doi.org/10.3390/en8054237>.
- [83] M. Ma, L. Ouyang, J. Liu, H. Wang, H. Shao, M. Zhu, Air -stable hydrogen generation materials and enhanced hydrolysis performance of MgH₂-LiNH₂ composites, *J. Power Sources* 359 (2017) 427–434, <https://doi.org/10.1016/j.jpowsour.2017.05.087>.